Acoustoelectric interaction of surface phonons in semiconductors. II. Effects of elastic anisotropy

Shin-ichiro Tamura
Department of Engineering Science, Hokkaido University, Sapporo 060, Japan
(Received 16 March 1979)

The acoustoelectric interaction of surface phonons with conduction electrons in piezoelectric semiconductors is investigated in the frequency region where the piezoelectric coupling is the predominant mode of interaction. We derive the interaction explicitly taking the elastic anisotropy of the semiconductors into account. The electronic state near the semiconductor surface, due to the presence of the surface space-charge layer, is also properly considered to specify the interaction. Applying the interaction to the study of the amplification characteristics of surface acoustic waves of GHz frequencies (propagated on the basal plane of a cubic crystal), we find that the elastic anisotropy reduces the interaction significantly compared with that of the isotropic approximation. Furthermore, when the wavelengths of the surface phonons become comparable to the width of the surface-depletion layer, the frequency dependence of the amplification rates suffers modifications also qualitatively.

I. INTRODUCTION

Recent experimental detections[1] of high-frequency (>10 GHz) sound waves which are excited thermally at the *surfaces* of solids seem to renew the interests in the interactions of surface phonons with various surface excitations. The interaction of surface phonons with conduction electrons near the surface of a piezoelectric semiconductor has been of theoretical interest from the viewpoint of the possible amplifications of surface acoustic waves (SAW's) in the GHz frequency region.[2] It might also attract our attention because the interaction is thought to be sensitive to the electrons in the vicinity of the surface and we may understand some properties of the electronic states in the surface space-charge layer of the semiconductor by investigating properly the interaction of the surface phonons with the electrons. In either case, we should initially obtain accurate solutions for the surface phonons of the semiconductor in the absence of interactions.

Recently, we have studied the acoustoelectric interaction of the surface phonons in the piezoelectric semiconductor.[3] In that work[3] (which we shall refer to as Paper I hereafter), the electronic states near the *n*-type semiconductor surface have been determined, though approximately, taking the bendings of the energy bands into account. Concerning the elastic properties of the semiconductor, however, we have assumed isotropy, that is, in Paper I the surface phonons are approximated as the quanta of the Rayleigh waves. The derived interaction of the surface phonons and the electrons based on the piezoelectric coupling is then applied to the study of the amplification characteristics of SAW's of GHz frequencies. Subsequently, it has been found that the frequency dependence of the surface-phonon-amplification rate is sensitive especially to the spatial decay profile of the electric potential induced piezoelectrically by the acoustic fields of the surface phonons.

In real crystalline semiconductors, elastic anisotropy is present to some extent. One of the important characteristics of the SAW introduced by elastic anisotropy, as against elastic isotropy, is that the decay constants of the waves which describe the exponential decreasing of the SAW amplitudes with the depth may be complex instead of real numbers, and therefore the particle displacement may decay oscillating away from a crystal surface.[4] Hence, the electric potential accompanying the SAW's in anisotropic crystals will also manifest itself as an oscillatory decay, whereas a rather monotonous decay takes place for the potential in isotropic crystals.[3,5] Consequently, as was commented in Paper I, anisotropy will have some effects on the interaction when discussed quantitatively.

The purpose of the present paper is to investigate the acoustoelectric interaction of the surface phonons in piezoelectric semiconductors taking elastic anisotropy into account. Like the case of Paper I, we shall derive the interaction assuming piezoelectric coupling between the surface phonons and conduction electrons, and then we shall predict the amplification characteristics of the SAW more quantitatively in the GHz frequency region. Here, it may be worthwhile to note that piezoelectric coupling is the dominant mode of the acoustoelectric interaction for phonons of frequencies lower than 10 GHz.[6]

The effects produced by the presence of the anisotropy on the theory of the acoustic waves are considerably complicated even when piezoelectricity is ignored, with the SAW's exhibiting diverse propagation

characteristics depending upon the crystal structure, the propagation direction, and the crystal plane on which they travel, and even on the values of the anisotropy ratio being greater or less than unity.[4] If piezoelectricity is taken into account, the modified SAW sometimes referred to as the piezoelectric surface waves or the electroacoustic surface waves could be propagated.[7–9] They are substantially characteristic in piezoelectric materials and are accompanied by electric fields. Some of these waves are reduced to bulk waves when the piezoelectric effect turns off. A typical example of such waves are the Bleustein waves in hexagonal crystals, which become SH waves (horizontally polarized shear waves) when piezoelectricity vanishes.[7] Similar waves have been reported to exist also in cubic crystals.[8] Moreover, it is known that there exist waves called pseudo surface waves (PSW's) which are not exact SAW's except at some isolated angles.[4] All these waves are important from the viewpoint of applications. In this paper, however, we again postulate weak piezoelectricity and treat the piezoelectric coupling as a perturbation on the acoustic fields. Therefore, the interaction of the piezoelectric surface waves which have no counterparts in nonpiezoelectric materials should be discussed separately.[10] The SAW's other than such piezoelectric surface waves and their quanta are the objects of our study.

In Sec. II, we briefly review the SAW's in the anisotropic, nonpiezoelectric, and homogeneous elastic continuum occupying the half space. Especially, the SAW's traveling on the basal plane of a cubic crystal (GaAs) are exemplified numerically in order to emphasize the distinction from the Rayleigh waves in isotropic media. The PSW's will also be considered only in an isolated direction on the plane where they become genuine surface waves. Hence, throughout this paper, the PSW's are to be understood as the true surface waves in the pseudo branch and we shall call the SAW's other than the PSW's the SAW's in the normal branch. In Sec. III, the phonon operators corresponding to the SAW's in the anisotropic medium are introduced. Although the complete orthonormal set of acoustic waves in the half space has not yet been constructed in the presence of elastic anisotropy, the relevant SAW solutions which form an orthonormal set are assumed to be members of the complete set. The electronic wave functions in n-type semiconductors are specified (approximately) in Sec. IV by taking the existence of the surface depletion layer into account. Section V is devoted to deriving the electron–surface-phonon interaction based on piezoelectric coupling, where piezoelectricity is assumed to act on the acoustic waves as a weak perturbation. The formula for the attenuation (or the amplification) rate of the surface phonons is presented in Sec. VI in the Born approximation. The effect of the finite relaxation time of the electrons will be neglected again in this paper. In Sec. VII, we develop numerical examples of the surface-phonon amplification for n-type GaAs at $T=77$ K and for 1–10-GHz phonon frequencies. The conclusions of this paper will be given in Sec. VIII.

II. SURFACE ACOUSTIC WAVES IN ANISOTROPIC MEDIA

Unlike the case of noncrystalline solids such as amorphous materials whose elastic properties may be approximated to be isotropic, real crystalline semiconductors have elastic anisotropy to some extent. For instance, the anisotropy ratios η defined as $\eta=2c_{44}/(c_{11}-c_{12})$ are 1.83 and 1.99 for GaAs and InSb of zinc-blende crystal structure, respectively,[11] while the ratio is unity for isotropic materials. As has been stated in the Introduction, the effects produced by the presence of anisotropy on SAW theory are considerably more complicated than those for isotropic media, and extensive computer calculations are generally required for their quantitative discussion.

The important characteristics of the SAW introduced by the anisotropy and relevant to this paper are summarized as follows: (i) The particle motion may include three independent orthogonal components, against just two for the Rayleigh-wave solution in isotropic media; (ii) the SAW velocity depends upon the direction of propagation; and (iii) the decay constants may be complex instead of real and then the particle displacement decays oscillating away from the surface, whereas it decays rather monotonously in isotropic media. Furthermore, it is known that the propagation vector of the SAW is not always collinear with the power flow.[4]

In order to make this paper self-contained, we shall briefly review the properties of the SAW mentioned above more quantitatively. First, let us set the Cartesian coordinate system so that the semiconductor extends over the half space $x_3>0$ and has the flat surface $x_3=0$ parallel to the x_1-x_2 plane. The wave equation for the particle displacement can be written, if no body forces and no piezoelectric effects are present,

$$\rho\ddot{u}_i=c_{ijkl}\partial_j\partial_k u_l=\partial_j T_{ij} \ , \tag{1}$$

where $\partial_i\equiv\partial/\partial x_i$, and u_i ($i=1$, 2, and 3) is the component of the displacement vector along the x_i axis. ρ, $\{c_{ijkl}\}$, and $\{T_{ij}\}$ are the mass density, the elastic-moduli tensor, and the stress tensor, respectively. Summation over repeated subscripts is assumed in Eq. (1).

We consider the solution of the wave equation (1) of the form

$$\vec{u}=\vec{a}\exp(ik\kappa_3 x_3)\exp[ik(\kappa_1 x_1+\kappa_2 x_2-vt)] \ , \tag{2}$$

where $\vec{a}$ is a constant vector, both κ_1 and κ_2 are real

numbers satisfying $\kappa_1^2+\kappa_2^2=1$ and k is the magnitude of the propagation vector parallel to the surface. The parameter κ_3 which takes a complex value determines the variation of the particle displacement with depth. Here, a displacement vector $\vec{u}$ of complex value has been assumed for calculational convenience. Either the real or the imaginary part of Eq. (2) should be understood as the real displacement. Since we are looking for the SAW solutions whose amplitudes are bounded in the neighborhood of a solid surface, κ_3 must have a positive imaginary part so that the displacement may vanish for $x_3 \to \infty$. Hence, Eq. (2) describes a wave damping in the x_3 direction and traveling with a phase velocity v in the x_1-x_2 plane along a direction fixed by the direction cosine (κ_1, κ_2).

Substituting Eq. (2) into Eq. (1), we have

$$(\rho v^2\delta_{il}-c_{ijkl}\kappa_j\kappa_k)a_l=0 \ , \tag{3}$$

or we have a secular equation,

$$\det(\rho v^2\delta_{il}-c_{ijkl}\kappa_j\kappa_k)=0 \ . \tag{4}$$

Equation (4) can be regarded as a sextic equation in κ_3 for the specified values of κ_1 and κ_2 with v as a parameter. However, only three roots out of six with positive imaginary parts are the desirable ones for our problem. For propagation of waves in a crystal plane of mirror symmetry or in certain high-symmetry directions on other planes of anisotropic media, one of the relevant roots lies on the imaginary axis and the other two form a pair symmetrically located with respect to the imaginary axis, i.e.,[4]

$$\kappa_3^{(1)}=\alpha+\beta i \ , \quad \kappa_3^{(2)}=-\alpha+\beta i \ ,$$

and

$$\kappa_3^{(3)}=\gamma i \ , \tag{5}$$

where β and γ are positive numbers. In what follows, we concentrate on such simple cases that the roots for κ_3 take the form of Eq. (5). It should be noted that for an isotropic medium, $\kappa_3^{(1)}$ and $\kappa_3^{(2)}$ are degenerate and become purely imaginary.

Corresponding to the three roots $\kappa_3^{(j)}$ given by Eq. (5), there exist three sets of eigenvectors $\vec{a}^{(j)}$ ($j=1$, 2, and 3) orthogonal to each other. Therefore, the correct SAW solutions of Eq. (1) consist of the linear combination of three terms like Eq. (2) with κ_3 given by Eq. (5), that is,

$$\vec{u}=\sum_{j=1}^{3}\vec{a}^{(j)}\exp(ik\kappa_3^{(j)}x_3)\exp[i(\vec{k}\cdot\vec{x}-\omega t)] \ , \tag{6}$$

where $\vec{k}=(k_1,k_2)=(k\kappa_1,k\kappa_2)$, $\vec{x}=(x_1,x_2)$, and $\omega=kv$. The relative magnitudes among $a_i^{(j)}$ ($i=1$, 2, and 3) for a given j or $\kappa_3^{(j)}$ are determined by Eq. (3). On the other hand, those among the $a_i^{(j)}$ ($j=1$, 2, and 3) for a fixed i, as well as the SAW velocity v, are determined only after the boundary conditions to be imposed on Eq. (1) are specified. The boundary conditions satisfied by a stress-free flat surface can be written

$$T_{i3}=c_{i3kl}\partial_k u_l=0 \ \text{ at } x_3=0 \quad (i=1,\ 2,\ \text{and } 3) \ . \tag{7}$$

Substituting Eq. (6) into Eq. (7) and expressing $a_1^{(j)}$ and $a_2^{(j)}$ in terms of the $a_3^{(j)}$ with the aid of Eq. (3) as stated above, we obtain another set of homogeneous equations in the $a_3^{(j)}$ for $j=1$, 2, and 3. Therefore, we also obtain a secular equation to be satisfied by the SAW velocity v. Finally, if an appropriate normalization condition is imposed on the displacement vector of the SAW, then $\vec{a}^{(j)}$, $\kappa_3^{(j)}$, and v are completely determined.

Here, we rewrite Eq. (6) using Eq. (5) so that we can see more explicitly the oscillatory damping of the particle motion in the x_3 direction away from the surface, i.e.,

$$\vec{u}_{\vec{k}}(\vec{r},t)=[(\vec{a}^{(+)}\cos\alpha kx_3+\vec{a}^{(-)}\sin\alpha kx_3)\exp(-\beta kx_3)+\vec{a}^{(3)}\exp(-\gamma kx_3)]\exp[i(\vec{k}\cdot\vec{x}-\omega t)]\equiv\vec{u}_{\vec{k}}(\vec{r})e^{-i\omega t} \ , \tag{8}$$

where $\vec{r}=(\vec{x},x_3)$, $\vec{a}^{(+)}=\vec{a}^{(1)}+\vec{a}^{(2)}$, and $\vec{a}^{(-)}=i(\vec{a}^{(1)}-\vec{a}^{(2)})$. If we normalize the displacement vector $\vec{u}_{\vec{k}}(\vec{r})$ by

$$\int d\vec{r}\,|\vec{u}_{\vec{k}}|^2=\int d\vec{x}\int_0^\infty dx_3\,|\vec{u}_{\vec{k}}|^2=1 \ , \tag{9}$$

the $\vec{a}$ coefficients result to be proportional to $(k/S)^{1/2}$, where S is the surface area, and hence it is convenient for further calculations to introduce the $\vec{b}$ vectors by

$$\vec{a}^{(j)}=(k/S)^{1/2}\vec{b}^{(j)} \ , \quad j=\pm \text{ and } 3 \ . \tag{10}$$

It should be noted that the factor $(k/S)^{1/2}$ in the displacement vector is the one to be compared with the factor $V^{-1/2}$ which appears for the normalization of the bulk waves, where V is the volume of the medium. The difference is due to the fact that in the half space the translation invariance in the x_3 direction is lost and it follows to introduce the factor $k^{1/2}$ for the SAW instead of $L^{-1/2}$ for the bulk waves, where L is the normalization length. The meaning of the normalization (9) adopted here will become clear in Sec. III.

Now, as for a simple example of the SAW traveling on an anisotropic medium, those on a cubic crystal with the basal plane as the free surface have been

computed numerically. We choose GaAs as a typical material and consider the propagation of the SAW on its surface. The piezoelectric effects are ignored in the calculations. The following set of parameters for the GaAs are used:

$$\rho = 5.32 \text{ g/cm}^3 ,$$

$$c_{11} = 1.188 \times 10^{12} \text{ dyne/cm}^2 ,$$

$$c_{12} = 0.538 \times 10^{12} \text{ dyne/cm}^2$$

and

$$c_{44} = 0.594 \times 10^{12} \text{ dyne/cm}^2 .$$

The anisotropy ratio is $\eta = 1.83$.[12]

Figure 1 shows the depth dependence of the particle displacement of the SAW traveling in the direction rotated by 5° away from the [100] axis on the (001) plane. For the SAW propagating along a crystal axis, the component u_T of the displacement vector normal to the sagittal plane (a plane containing the wave vector and perpendicular to the surface) vanishes and the remaining two components u_L and u_V have finite values just as in the case of Rayleigh waves, where u_L is measured along the propagation vector $\vec{k}$ and u_V is normal to the free surface. However, u_T begins to grow as the vector $\vec{k}$ is rotated away from the crystal axis. In Fig. 1, we can actually see the small but finite value of u_T other than the characteristic oscillatory damping of the particle displacement.[13]

In order to see these points more in detail, the various components of the relative surface displacement of the SAW for propagation in the (001) plane are drawn in Fig. 2. The solid curves give the sum of the contributions from the terms including the pair of roots $\kappa_3^{(1)}$ and $\kappa_3^{(2)}$, that is, the coefficients of the cosine terms of Eq. (8), while the broken curves show the surface displacements due to the term with the pure imaginary root $\kappa_3^{(3)}$. We immediately find the elliptical particle motions in the sagittal plane for $\vec{k}$ parallel to the [100] direction. We can also see how the component u_T grows according to the direction of the wave vector. For propagation in the [110] direction the waves of the normal branch are reduced to be purely transverse in the plane parallel to the surface, i.e., $u_L = u_V = 0$. However, the waves traveling in this direction on the (001) plane do not localize their amplitudes in the neighborhood of the surface but rather are bulk waves. This can be understood by investigating the angle dependence of the decay parameters, which are shown in Fig. 3.

Figure 3 illustrates the variations of the real and the imaginary parts of the solutions κ_3 as functions of angle in the (001) plane. Both α and β have finite values throughout this plane, whereas γ decreases gradually as the angle of the wave vector away from the crystal axis increases, and it vanishes at 45°. Consequently, the SAW's of the normal branch degenerate into bulk transverse waves (SH waves) for

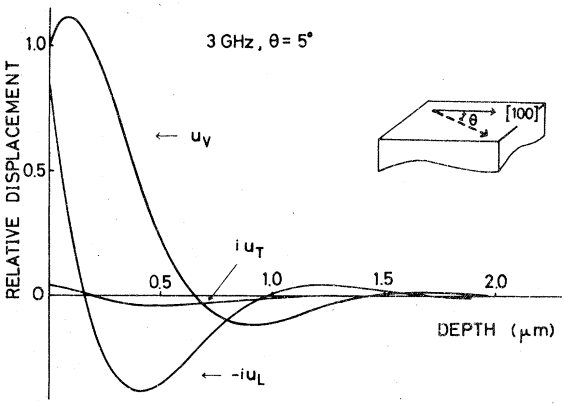

FIG. 1. Depth dependence of longitudinal, transverse, and vertical displacement of SAW's for 3-GHz frequency. The propagation direction is rotated 5° away from the [100] axis on (001) plane of GaAs.

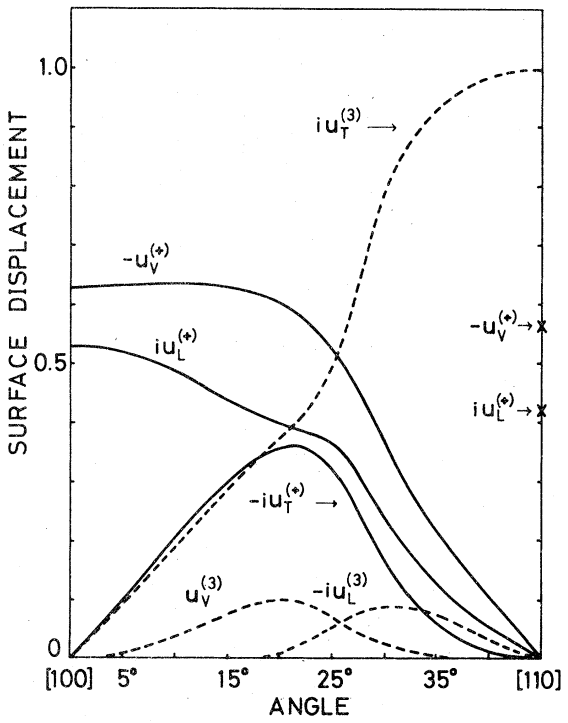

FIG. 2. Relative magnitude of various components of the surface displacement. The solid curves are sums of contributions of terms with pair roots conjugate to each other and the broken curves are for the term with pure imaginary root. For PSW's, components other than $u_{V,L}^{(+)}$ (crosses at 45°) are zero. It should be noted that the surface displacement of this figure is calculated based on the normalization $\sum_{j=1}^{3} |\bar{a}^{(j)}|^2 = 1$ instead of the normalization of Eq. (9).

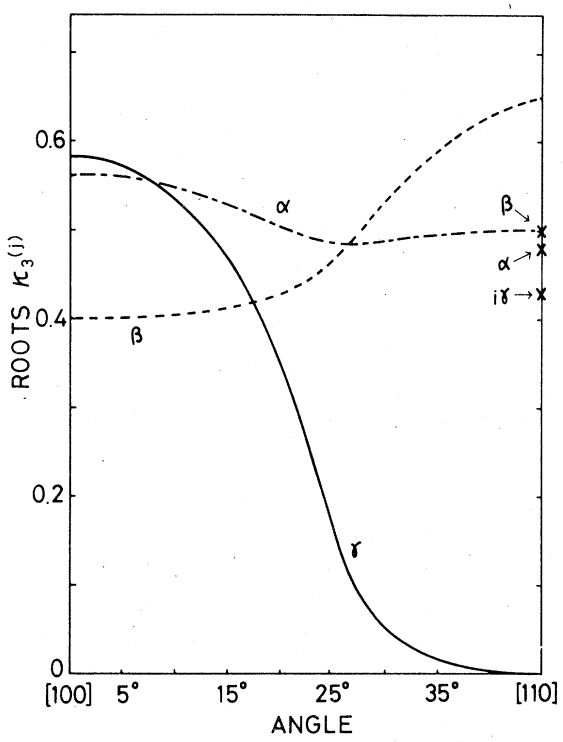

FIG. 3. Variation of roots $\kappa_3^{(j)}$. $\alpha = \mathrm{Re}\kappa_3^{(1)} = -\mathrm{Re}\kappa_3^{(2)}$, $\beta = \mathrm{Im}\kappa_3^{(1)} = \mathrm{Im}\kappa_3^{(2)}$, and $\gamma = \mathrm{Im}\kappa_3^{(3)}$. For PSW's (crosses at 45°), $\kappa_3^{(3)}$ is purely real and $\kappa_3^{(3)} < 0$.

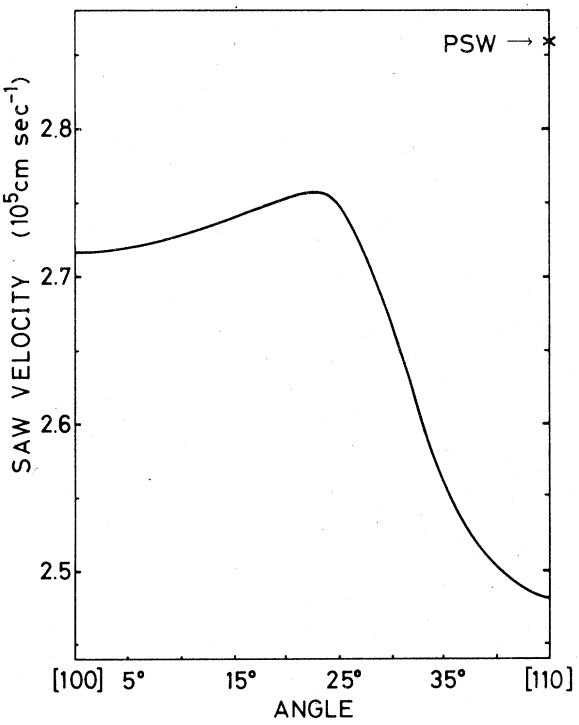

FIG. 4. SAW velocities for propagation on the (001) plane of GaAs.

propagation right along the [110] direction.

In the direction where the SAW's of the normal branch become bulk waves, the other SAW solutions, or the PSW's appear. In Fig. 2, we have also shown by the crosses the components of the surface displacement for the PSW. As can be seen, the PSW's are the Rayleigh-type ones, that is, the particle displacement is elliptic in the sagittal plane. From Fig. 3, we note that the root $\kappa_3^{(3)}$ of the PSW is purely real but the corresponding eigenvector $\vec{a}^{(3)}$ is identically zero and it does not contribute to the waves.[4]

Finally, Fig. 4 displays the magnitude of the phase velocity of the SAW on the (001) plane. The local maximum of the velocity is attained at an angle close to 22.5°. The directions in which the velocity takes on its extreme values are known as the pure-mode axes, that is, both the phase and the group velocities become collinear.[4] Incidentally, note that the PSW's travel much faster than the slowest SH waves in the same direction and any other SAW's on the same crystal surface.

III. SURFACE PHONON

In Sec. II, the SAW solutions in the anisotropic medium have been recapitulated by considering a cubic crystal as the simplest example of such a medium. In the following, we shall concentrate on the interaction of surface phonons with the conduction electrons in semiconductors. Hence, here we introduce the phonon operators corresponding to the SAW in the homogeneous anisotropic medium.

For the sake of convenience, let us define the operator $\tilde{L}(\partial)$ by writing the equation of motion (1)

$$\rho \ddot{u}_i = \tilde{L}(\partial)_{ij} u_j \ , \tag{11}$$

and consider the following quantity:

$$(\vec{u}, \tilde{L}\,\vec{u}) \equiv \int u_i \tilde{L}(\partial)_{ij} u_j \, d\vec{r} \ . \tag{12}$$

Recalling the fact that the integration is carried out over the half space, we have

$$(\vec{u}, \tilde{L}\,\vec{u}) = -c_{ijkl} \int \partial_j u_i \partial_k u_l \, d\vec{r} + \int u_i T_{i3} \, d\vec{x}\,|_{x_3=0} \ . \tag{13}$$

It should be noted that the second term of the right-hand side of Eq. (13) vanishes due to the boundary condition (7).

Now, the equation of motion (1) is derivable from the Lagrangian

$$L = \int (\tfrac{1}{2}\rho \dot{u}_i \dot{u}_i - \tfrac{1}{2} c_{ijkl} \partial_j u_i \partial_k u_l) \, d\vec{r} \tag{14}$$

and then we have the Hamiltonian of the system,

$$H=\int\left[\frac{1}{2\rho}\pi_i\pi_i+\frac{1}{2}c_{ijkl}\partial_j u_i\partial_k u_l\right]d\vec{r}\ , \tag{15}$$

where $\pi_i=\rho\dot{u}_i$. Owing to Eq. (13), it can be seen that the Hamiltonian takes the form

$$H=1/2\rho(\vec{\pi},\vec{\pi})-\tfrac{1}{2}(\vec{u},\tilde{L}\,\vec{u})\ . \tag{16}$$

For the time being, we again allow $\vec{u}$ to be complex valued and put its time evolution by the exponential factor $\exp(-i\omega_Q t)$ as follows:

$$\vec{u}=\vec{u}_Q(\vec{r})\exp(-i\omega_Q t)\ , \tag{17}$$

where Q stands for a set of possible quantum numbers specifying the eigenmodes of the acoustic waves in the half space, that is, both surface and bulk in character. Accordingly, Eq. (11) is reduced to the eigenvalue equation formally written

$$-\tilde{L}(\partial)\,\vec{u}_Q(\vec{r})=\rho\omega_Q^2\,\vec{u}_Q(\vec{r})\ . \tag{18}$$

In the linear space of the acoustic waves satisfying the boundary condition, the operator $\tilde{L}(\partial)$ is Hermitian and we have for the eigenwaves $\vec{u}_Q$ the orthogonality relation of the form

$$\langle u_Q,u_{Q'}\rangle\equiv\int[\vec{u}_Q(\vec{r})]^*\cdot\vec{u}_{Q'}(\vec{r})\,d\vec{r}=0\ , \tag{19}$$

if

$$\omega_Q\neq\omega_{Q'}\ .$$

Here, we shall normalize $\vec{u}_Q$ according to

$$\langle\vec{u}_Q,\vec{u}_Q\rangle=1\ , \tag{20}$$

where the sum should not be taken for the subscript Q. Furthermore, if we make the displacement vector real valued by adding the complex conjugate of Eq. (17) to itself,

$$\vec{v}_Q(\vec{r},t)=\vec{u}_Q(\vec{r})\exp(-i\omega_Q t)+[\vec{u}_Q(\vec{r})]^*\exp(i\omega_Q t)\ , \tag{21}$$

$\vec{v}_Q$ also satisfies Eq. (18) with $\vec{u}_Q$ replaced by $\vec{v}_Q$. Therefore, it is concluded again that

$$\langle\vec{v}_Q,\vec{v}_{Q'}\rangle=0\ ,\quad \text{if } \omega_Q\neq\omega_{Q'}\ . \tag{22}$$

Decomposing Eq. (22) with the aid of Eq. (19), we obtain the following relation for $\omega_Q\neq\omega_{Q'}$:

$$(\vec{u}_Q,\vec{u}_{Q'})\exp[-i(\omega_Q+\omega_{Q'})t]+(\vec{u}_Q^{\,*},\vec{u}_{Q'}^{\,*})\exp[i(\omega_Q+\omega_{Q'})t]=0\ . \tag{23}$$

Since the two exponential functions in the above expression are linearly independent, Eq. (23) yields

$$(\vec{u}_Q,\vec{u}_{Q'})=(\vec{u}_Q^{\,*},\vec{u}_{Q'}^{\,*})=0\ ,\quad \text{if } \omega_Q\neq\omega_{Q'}\ . \tag{24}$$

This result will be used later to derive Eq. (29).

Provided that the orthonormal set of eigenwaves $\{\vec{u}_Q(\vec{r})\}$ in the half space is complete, the displacement vector $\vec{u}(\vec{r},t)$ of the medium can be expanded as follows by taking its being real into account

$$\vec{u}(\vec{r},t)=\sum_Q\left(\frac{\hbar}{2\rho\omega_Q}\right)^{1/2}[a_Q\vec{u}_Q(\vec{r})\exp(-i\omega_Q t)+a_Q^\dagger\vec{u}_Q^{\,*}(\vec{r})\exp(i\omega_Q t)]\ . \tag{25}$$

Similarly, for the momentum $\vec{\pi}$ canonically conjugate to $\vec{u}$, we have

$$\vec{\pi}(\vec{r},t)=-i\sum_Q\left(\frac{\hbar\rho\omega_Q}{2}\right)^{1/2}[a_Q\vec{u}_Q(\vec{r})\exp(-i\omega_Q t)-a_Q^\dagger\vec{u}_Q^{\,*}(\vec{r})\exp(i\omega_Q t)]\ , \tag{26}$$

where a_Q and $a_Q^\dagger$ are the annihilation and creation operators of the Q-mode phonons satisfying the commutation relations

$$[a_Q,a_{Q'}^\dagger]=\delta_{QQ'},\quad [a_Q,a_{Q'}]=[a_Q^\dagger,a_{Q'}^\dagger]=0\ . \tag{27}$$

Equation (27) is derived from the canonical commutation relations satisfied by $\vec{u}$ and $\vec{\pi}$ and the assumed completeness relation

$$\sum_Q u_Q^l(\vec{r})[u_Q^{l'}(\vec{r}')]^*=\delta_{ij}\delta(\vec{r}-\vec{r}')\ . \tag{28}$$

Now, substituting Eqs. (25) and (26) into Eq. (16) and noting Eq. (24), the Hamiltonian is calculated to be

$$H=\sum_Q\hbar\omega_Q(a_Q^\dagger a_Q+\tfrac{1}{2})\ . \tag{29}$$

At this stage, a_Q and $a_Q^\dagger$ can be understood as the correct phonon operators specified by the quantum numbers Q.

In order to quantize the relevant SAW's in this paper, we must expand the particle displacement associated with the SAW in terms of the complete orthonormal set $\{\vec{u}_Q\}$ of the eigenwaves in the homogeneous but anisotropic half space. Unfortunately, such a complete orthonormal set has not yet been constructed for the anisotropic medium. However, if we consider the SAW's traveling on a given crystal surface, as have been seen in Sec. II, we find that they form an orthonormal set of waves with respect to the wave vector $\vec{k}$ parallel to the surface, that is,

$$\langle\vec{u}_{\vec{k}},\vec{u}_{\vec{k}'}\rangle=0\ ,\quad \text{if } \vec{k}\neq\vec{k}' \tag{30}$$

and

$$\langle\vec{u}_{\vec{k}},\vec{u}_{\vec{k}}\rangle=1\ . \tag{31}$$

The orthogonality with respect to the two-dimensional wave vector parallel to the surface holds also for the bulk waves in the half space as far as waves of the form $e^{i\vec{k}\cdot\vec{x}}\vec{w}_{\vec{k}}(x_3)$ ($\vec{k}$ real) satisfying translation invariance in the x_1-x_2 plane are concerned. Therefore, one of the quantum numbers which specifies the eigenwaves in the half space must be the wave vector $\vec{k}$ parallel to the surface and we may write $Q=(\lambda,\vec{k},\cdots)$, where λ denotes the polarization of the waves and the dots indicate other possible quantum numbers. Here, we note that the wave vector $\vec{k}$ is the only quantum number for the SAW, because once it is specified the SAW solutions are uniquely determined. Furthermore, if we remember the dispersion relation of the acoustic waves, which can be written as $\omega(\vec{k})=v(\vec{k}/k)k$, we may choose quantum numbers such as $Q=(\lambda,\omega,v,\cdots)$, instead of $Q=(\lambda,\vec{k},\cdots)$. The velocity v of the SAW's is known to be slower than for the slowest bulk waves propagating in the same direction as the SAW's except for certain isolated directions, for instance, the [110] direction on the (001) plane. There the SAW's of the normal branch reduce to the bulk SH waves and the PSW's with velocity faster than that of the SH waves appear. Hence, the SAW solutions $\{\vec{u}_{\vec{k}}(\vec{r})\}$ of Eq. (8) on the (001) plane are orthogonal to other eigenwaves of the bulk modes in the half space except at 45°, because there exists no overlapping in their velocities. Moreover, bulk waves in a half space which have a velocity distribution overlapping the PSW velocity would be only SH waves, since the slowest SV waves (shear waves with vertical polarization) travel faster than the PSW's.[4] However, the PSW's are polarized in the sagittal plane whereas the SH waves are polarized normal to it. Therefore, the PSW's will be orthogonal to the bulk waves as well.

Accordingly, we may convince ourselves that for propagation on the (001) plane, the SAW solutions $\{\vec{u}_{\vec{k}}(\vec{r})\}$ form an orthonormal set of acoustic waves together with the translation-invariant bulk waves in the half space.[14] Furthermore, since the solutions of the wave equation discussed so far belong to the linear space in which the operator $\tilde{L}(\partial)$ satisfies Hermiticity, the assumed orthonormal set must be complete. Then, we expand the displacement vector $\vec{u}(\vec{r},t)$ accompanying the SAW as follows:

$$\vec{u}(\vec{r},t)=\sum_{\vec{k}}\left(\frac{\hbar}{2\rho\omega_k}\right)^{1/2}[a_{\vec{k}}\vec{u}_{\vec{k}}(\vec{r})\exp(-i\omega_k t)+a_{\vec{k}}^{\dagger}\vec{u}_{\vec{k}}^{*}\exp(i\omega_k t)] \quad , \tag{32}$$

where $a_{\vec{k}}^{\dagger}$ and $a_{\vec{k}}$ are the creation and annihilation operators of the surface phonons (quanta of the SAW) which satisfy the commutation relations (27), with $Q=\vec{k}$. The normalization condition (9) for $\vec{u}_{\vec{k}}$ is idential to Eq. (20) and it upholds the Hamiltonian becoming of the form of Eq. (29).

IV. ELECTRONIC STATES

In order to specify the interaction of the surface phonons with the electrons, we must know the electronic states near the semiconductor surface in the absence of acoustic disturbance. The electronic states in the vicinity of the semiconductor surface are different from those of the bulk region due to the presence of a space-charge region and the potential barrier associated with it.[15] In the n-type semiconductor in which we shall be interested, some of the electrons in the conduction band are trapped by the acceptor-like surface states and a positive-space-charge layer (called a surface depletion layer) is generally formed adjacent to the surface. Therefore, in the neighborhood of the surface, energy bands bend upward with respect to the Fermi level.

The surface-charge density and the shape of the potential barrier are obtained by solving the Poisson equation under appropriate boundary conditions. The electronic states are then determined by solving the Schrödinger equation with the potential obtained in this manner. In the simplest approximation, the potential is solved to be a semiquadratic function of the depth and makes a barrier of Schottky-type, that is,[3]

$$V=\frac{2\pi e^2 n}{\epsilon_0}(l_0-x_3)^2\Theta(l_0-x_3) \quad , \tag{33}$$

with

$$\Theta(x)=\begin{cases}1 & \text{for } x\geq 0 \ , \\ 0 & \text{for } x<0 \ , \end{cases} \tag{34}$$

where ϵ_0 and n are the static dielectric constant and the bulk electron concentration, respectively. The coordinate system is chosen to be the same as that in Sec. II, that is, the semiconductor extends over the half space $x_3>0$. In Eq. (33), the parameter l_0 measures the width of the depletion layer and is determined by the bulk electron concentration and the band bending at the free surface, $e\phi_s$, as

$$l_0=\left(\frac{\epsilon_0\phi_s}{2\pi e n}\right)^{1/2} \quad . \tag{35}$$

The potential (33) is derived assuming that there are no electrons in the depletion layer $x<l_0$.

The motion of the electrons in the vicinity of the n-type semiconductor surface can be characterized by wave functions of the form

$$\Phi_{\vec{p},q}(\vec{r})=e^{i\vec{p}\cdot\vec{x}}\psi_q(x_3) \quad , \tag{36}$$

where $\vec{p}=(p_1,p_2)$ is the wave vector of the electrons parallel to the surface and the wave function $\psi_q(x_3)$ is governed by the Schrödinger equation

$$\left(-\frac{\hbar^2}{2m}\frac{d^2}{dx_3^2}+V(x_3)\right)\psi_q(x_3)=\epsilon_q\psi_q(x_3) \quad , \tag{37}$$

where m is the electron effective mass (assuming a spherical constant-energy surface) and the energies of the electrons are given by

$$E_{\vec{p},q}=\hbar^2\vec{p}^2/2m+\epsilon_q \quad . \tag{38}$$

In this paper, the Schrödinger equation (37) will be solved with the approximate potential of Eq. (33). While the self-consistent equations for the potential and the electron wave function near the semiconductor surface are easily found by adding an equation which combines both quantities, it is very hard to solve them even numerically, unlike the case of electrons in a surface inversion layer.[16]

Equation (37) with the potential (33) cannot still be solved exactly but has a fairly good approximate solution which may be expressed analytically. Such a solution is[3]

$$\psi_q(x_3)=\begin{cases} B_q\left(\dfrac{\xi_q}{P_q}\right)^{1/2}[J_{1/3}(\xi_q)+J_{-1/3}(\xi_q)] \quad , \\ \qquad\qquad \text{for } x_3\geq a \quad , \\ B_q\left(\dfrac{\eta_q}{P_q}\right)^{1/2}[I_{1/3}(\eta_q)-I_{-1/3}(\eta_q)] \quad , \\ \qquad\qquad \text{for } x_3<a \quad , \end{cases} \tag{39}$$

with

$$B_q=-(\pi q/3L)^{1/2},\ \epsilon_q=\hbar^2q^2/2m, \tag{40}$$

$$P_q(x_3)=[2m|\epsilon_q-V(x_3)|]^{1/2}/\hbar \quad ,$$

$$\xi_q(x_3)=\int_a^{x_3}P_q(z)\,dz \quad \text{for } x_3\geq a \quad , \tag{41}$$

and

$$\eta_q(x_3)=\int_{x_3}^{a}P_q(z)\,dz \quad \text{for } x_3<a \quad , \tag{42}$$

where a denotes the classical turning point defined by $\epsilon_q=V(a)$, L is the thickness of the semiconductor, and J_ν and I_ν are the Bessel functions of real and imaginary arguments, respectively. For a semi-infinite semiconductor ($L\gg l_0$), the wave number q takes continuous positive values. ξ and η can be explicitly integrated to be

$$\xi_q(x_3)=\begin{cases} \dfrac{\epsilon_q}{\hbar\omega_0}[\sin^{-1}t+t(1-t^2)^{1/2}+\frac{1}{2}\pi] \\ \qquad\qquad \text{for } a<x_3<l_0 \quad , \\ \dfrac{\epsilon_q}{\hbar\omega_0}(2t+\frac{1}{2}\pi) \quad \text{for } x_3>l_0 \end{cases} \tag{43}$$

and

$$\eta_q(x_3)=\frac{\epsilon_q}{\hbar\omega_0}[\ln t+(t^2-1)^{1/2}-t(t^2-1)^{1/2}] \quad , \tag{44}$$

where $\omega_0^2=4\pi e^2n/m\epsilon_0$ is the square of the plasma frequency and $t=(m\omega_0^2/2\epsilon_q)^{1/2}(x_3-l_0)$.

The electron density calculated from the wave function (39) has finite values for $x_3<l_0$, contrary to the assumption on which basis Eq. (33) has been derived.

Finally, we introduce the wave function $\Psi(\vec{r})$ of the electrons in second-quantized version by

$$\Psi(\vec{r})=\frac{1}{\sqrt{S}}\sum_{\vec{p},q}c_{\vec{p},q}\psi_q(x_3)e^{i\vec{p}\cdot\vec{x}} \quad , \tag{45}$$

where $c_{\vec{p},q}$ and its Hermitian conjugate $c^\dagger_{\vec{p},q}$ are annihilation and creation operators of the electrons which satisfy commutation relations of the Fermi-type.

V. INTERACTION

In the piezoelectric semiconductor, the conduction electrons interact with the surface phonons through piezoelectricity. They also interact with the surface phonons through the deformation potential which is proportional to the dilatation caused by the acoustic vibrations associated with the phonons. Although at very high acoustic-wave frequencies the deformation potential becomes the dominant mode of the acoustoelectric interaction even for the piezoelectric semiconductor, it can be neglected compared to piezoelectric coupling for frequencies from 1 to 10 GHz to be considered later in this paper. Hence, in what follows we exclusively concentrate on the piezoelectric interaction between the electrons and the surface phonons.

The relevant component of the piezoelectric fields induced in the semiconductor is derived from the piezoelectric equations of state for the acoustic and the electromagnetic fields together with the Maxwell equations in the electrostatic approximation, which are supplemented by the continuity equation of the charge. Here, we note that the variation of the sound velocities due to piezoelectric stiffening will be discarded because it amounts to only a small correction for the semiconductor considered in this work ($\Delta v/v\sim10^{-4}$ for GaAs), and the effects of the mobile charges in the semiconductor will be incorporated as electronic screening.

The piezoelectric potential ϕ produced by the propagation of the surface phonons satisfies the equation

$$\Delta\phi=\frac{2\pi}{\epsilon_0}e_{ijk}\partial_i(\partial_ju_k+\partial_ku_j) \quad , \tag{46}$$

for $\{e_{ijk}\}$ is the piezoelectric tensor and dielectric iso-

tropy has been assumed. Then, if we put

$$\vec{u}=\vec{a}\exp(ik\kappa_3 x_3+i\vec{k}\cdot\vec{x}) \tag{47}$$

and

$$\phi=d\exp(ik\kappa_3 x_3+i\vec{k}\cdot\vec{x}) \ , \tag{48}$$

it follows for crystals with zinc-blende crystal structure ($e_{14}=e_{25}=e_{36}=e_p$ and the other components vanish)

$$d=\frac{8\pi e_p}{\epsilon_0(1+\kappa_3^2)k^2}[k_1k_2a_3+\kappa_3k(k_1a_2+k_2a_1)] \ . \tag{49}$$

Therefore, the SAW's of Eq. (8) are accompanied by the electric potential[17]

$$\phi_{\vec{k}}(\vec{r},t)=-\frac{8\pi e_p}{\epsilon_0}k^{1/2}[(d^{(+)}\cos\alpha kx_3+d^{(-)}\sin\alpha kx_3)\exp(-\beta kx_3)+d^{(3)}\exp(-\gamma kx_3)]\exp[i(\vec{k}\cdot\vec{x}-\omega t)]\equiv\phi_{\vec{k}}(\vec{r})e^{-i\omega t} \ , \tag{50}$$

with

$$\begin{aligned} d^{(+)}&=D[(\beta^2-\alpha^2-1)F_1+2\alpha\beta F_2] \ , \\ d^{(-)}&=D[(\beta^2-\alpha^2-1)F_2-2\alpha\beta F_1] \ , \\ d^{(3)}&=\frac{1}{\gamma^2-1}[\kappa_1\kappa_2 b_3^{(3)}+i\gamma(\kappa_1 b_2^{(3)}+\kappa_2 b_1^{(3)})] \ , \end{aligned} \tag{51}$$

where

$$\begin{aligned} D&=[(\beta^2-\alpha^2-1)^2+4\alpha^2\beta^2]^{-1} \ , \\ F_1&=\kappa_1\kappa_2 b_3^{(+)}+i\kappa_1(b_2^{(+)}\beta-b_2^{(-)}\alpha) \\ &\quad +i\kappa_2(b_1^{(+)}\beta-b_1^{(-)}\alpha) \ , \\ F_2&=\kappa_1\kappa_2 b_3^{(-)}+i\kappa_1(b_2^{(+)}\alpha+b_2^{(-)}\beta) \\ &\quad +i\kappa_2(b_1^{(+)}\alpha+b_1^{(-)}\beta) \ . \end{aligned} \tag{52}$$

Figure 5 exhibits for GaAs the variation with angle of the d coefficients which appear in the induced potential. We observe that at 0°, all coefficients vanish so that the SAW's traveling along the crystal axis on the (001) plane of the cubic crystal are piezoelectrically inactive. At 45°, we also see that the SH waves are piezoelectrically inactive, whereas the PSW's are strongly active. These results may be elucidated with the help of Eqs. (51) and (52). At 0°, $\kappa_1=1$ and $\kappa_2=0$, and then we have

$$\begin{aligned} F_1&=i(b_2^{(+)}\beta-b_2^{(-)}\alpha) \ , \\ F_2&=i(b_2^{(+)}\alpha+b_2^{(-)}\beta) \ , \\ d^{(3)}&\propto b_2^{(3)} \ . \end{aligned} \tag{53}$$

Similarly, at 45°, $\kappa_1=\kappa_2=1/\sqrt{2}$ and we have

$$\begin{aligned} F_1&=\tfrac{1}{2}b_3^{(+)}+i(b_L^{(+)}\beta-b_L^{(-)}\alpha) \ , \\ F_2&=\tfrac{1}{2}b_3^{(-)}+i(b_L^{(+)}\alpha+b_L^{(-)}\beta) \ , \\ d^{(3)}&\propto\tfrac{1}{2}b_3^{(3)}+i\gamma b_L^{(3)} \ , \end{aligned} \tag{54}$$

where $b_L=(1/\sqrt{2})(b_1+b_2)$ is measured along the wave vector. Therefore, the only components of the waves polarized perpendicular to and parallel to the sagittal plane are piezoelectrically active at 0° and 45°, respectively. However, such components are not present at 0°, or in the [100] direction. On the other hand, in the [110] direction, the PSW's which are polarized in the sagittal plane have strong piezoelectric effects, whereas no such effects exist for the SH waves. It may be worthwhile to remember that, in the isotropic approximation, the SAW's traveling in the [100] direction of the cubic crystal have no piezoelectric effect either, but those propagating along the [110] direction couple to the piezoelectric field most strongly.

Next, examples of the spatial variation of the induced electric potential with depth are shown in Fig. 6. We immediately recognize the oscillatory damping of the potential, like that of the particle displacement. Comparing these spatial behaviors with the much simpler decay profile of the potential in isotropic materials, we find that the observed oscillation is again characteristic in media with anisotropy and will pro-

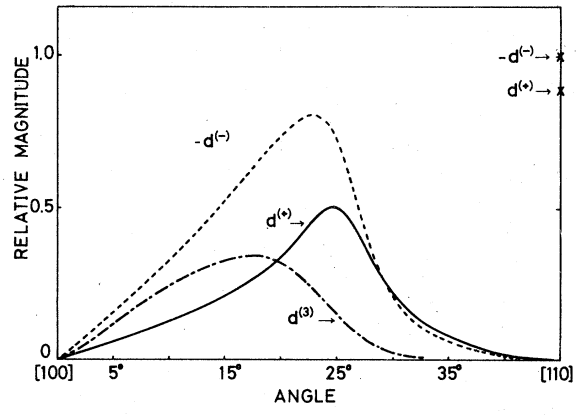

FIG. 5. Relative magnitude of the coefficients which appear in the induced potential [see Eqs. (50) and (51).] For PSW's $d^{(3)}=0$.

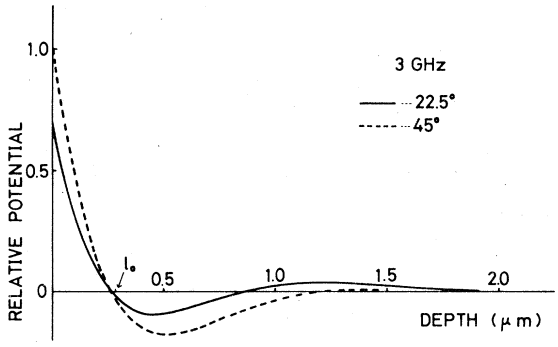

FIG. 6. Variation of the electric potentials with depth for 3-GHz phonon frequency. The solid and broken curves represent the variation for propagation rotated 22.5 and 45° (PSW), respectively, away from the [100] axis in the (001) plane.

duce results on the surface-phonon amplification rate qualitatively distinguishable from those of the isotropic approximation.

Now, in the phonon picture, the displacement vector of the SAW has been expanded as Eq. (32). Then, it is seen that the induced electric potential is quantized as follows:

$$\phi(\vec{r},t)=\sum_{\vec{k}}\left(\frac{\hbar}{2\rho\omega}\right)^{1/2}[a_{\vec{k}}\phi_{\vec{k}}(\vec{r},t)+a_{\vec{k}}^{\dagger}\phi_{\vec{k}}^{*}(\vec{r},t)]\ . \tag{55}$$

Taking these results into account, the interaction Hamiltonian of the surface phonons with the electrons in the semiconductor can be written

$$H_I=-e\int\Psi^{\dagger}(\vec{r})\phi(\vec{r},0)\Psi(\vec{r})\,d\vec{r}=\frac{8\pi e_p e}{\epsilon_0}\sum_{\vec{p},\vec{k}}\sum_{q',q}c_{\vec{p}+\vec{k},q'}^{\dagger}c_{\vec{p},q}a_{\vec{k}}\Xi_{q'q}(\vec{k})+\text{H.c.}\ , \tag{56}$$

where

$$\Xi_{q'q}(\vec{k})=\left(\frac{\hbar}{2\rho v}\right)^{1/2}\int_0^{\infty}\psi_{q'}^{*}(x_3)[(d^{(+)}\cos\alpha kx_3+d^{(-)}\sin\alpha kx_3)\exp(-\beta kx_3)+d^{(3)}\exp(-\gamma kx_3)]\psi_q(x_3)\,dx_3\ . \tag{57}$$

VI. ATTENUATION RATE OF SURFACE PHONON

During propagation on the semiconductor surface, the surface phonons are attenuated or amplified owing to their absorption or emission by the conduction electrons. This can be described basically by the Hamiltonian (56). However, correct understanding of the attenuations (or the amplifications) of the surface phonons except in the regime $kl \gg 1$ (l is the mean free path of the electrons) requires still additional knowledge on the finite lifetime of the electrons which may be produced by (56) as well as by other mechanisms.

In this paper, we shall employ the lowest-order approximation of perturbation theory to evaluate the attenuation rate of the surface phonons. This is because, as has been remarked in Paper I, for phonon frequencies larger than 1 GHz, $kl > 1$ holds and the effect of the relaxation time of the electrons plays an important role only at frequencies around 1 GHz.

Then, according to the golden rule, the width Γ of the surface phonons will be

$$\Gamma=\frac{2\pi}{\hbar}\sum_f|\langle f|H_I|i\rangle|^2\delta(E_f-E_i)\ , \tag{58}$$

which becomes, upon limiting it to phonons with two-dimensional wave vector $\vec{k}$ and energy $\hbar\omega$,

$$\Gamma_{\vec{k}}=\frac{2\pi}{\hbar}\left(\frac{8\pi e_p e}{\epsilon_0\epsilon(k)}\right)^2 N_k\sum_{\vec{p}}\sum_{q'q}(f_{\vec{p},q}-f_{\vec{p}+\vec{k},q'})|\Xi_{q'q}(\vec{k})|^2\delta(E_{\vec{k}+\vec{p},q'}-E_{\vec{p},q}-\hbar\omega)\ , \tag{59}$$

where N_k is the occupation number of the surface phonons and $f_{\vec{p},q}=f(E_{\vec{p},q})$ is the distribution function of the electrons. In this expression, we have introduced the static dielectric function $\epsilon(k)=1+(k_s/k)^2$ which expresses the screening of the piezoelectric fields by the electrons, where k_s is the reciprocal of the screening length.

If the attentuation rate α of the surface phonons is defined as $\Gamma_{\vec{k}}$ divided by the phonon flux $N_k v$, then it follows, after carrying out the sums over $\vec{p}$ and the electron spin,

$$\alpha_{\vec{k}}=-\frac{2m\omega}{\pi\hbar^2 v}\left(\frac{8\pi e_p e}{\epsilon_0\epsilon(k)}\right)^2\sum_{q'q}|\Xi_{q'q}(\vec{k})|^2\int dE\,\frac{df(E+\epsilon_q)}{dE}\left[\frac{2\hbar^2k^2}{m}E-\left(\epsilon_{q'}-\epsilon_q+\frac{\hbar^2k^2}{2m}-\hbar\omega\right)^2\right]^{-1/2}\ , \tag{60}$$

where the integration over E should be performed in the whole region where the argument of the square root is non-negative. Because df/dE is negative definite, the α defined by Eq. (60) is positive and the surface phonons are attenuated by the interaction with the electrons. In the presence of the dc electric field, however, a displaced distribution must be used for the electrons. If the electrons have a drift velocity v_d in the direction parallel to the wave vector $\vec{k}$ of the surface phonons, the frequency ω is to be replaced by $-\omega x$ in Eq. (60), where x is the so-called drift parameter defined by $x = v_d/v - 1$. Therefore, the attenuation rate α changes its sign from positive to negative as the electron drift velocity v_d exceeds the phonon velocity v and amplification of the surface phonons is attained.

VII. NUMERICAL RESULTS

As a numerical example, n-type GaAs with a bulk-electron mobility $\mu = 1.70 \times 10^4$ cm^2/V sec is considered at $T = 77$ K. This value of the mobility corresponds to the value of the bulk-electron concentration $n = 1.07 \times 10^{16}$ cm^{-3}. The piezoelectric and the dielectric constants are $e_p = 4.71 \times 10^4$ esu/cm^2 and $\epsilon_0 = 12.9$, respectively, and the electron effective mass is $m = 0.07 m_0$, where m_0 is the mass of the free electron. Combining these values with the band bending $e\phi_s = 0.59$ eV at the surface, the thickness of the depletion layer is computed to be $l_0 = 0.283$ μm.

The electronic screening will be considered in the Debye approximation in which the difference between the electronic motions parallel and perpendicular to the surface, as well as in the electron concentration in $x_3 < l_0$, is neglected. This is the same approximation made in the Paper I. In this case, we have the screening wave number $k_s = 4.75 \times 10^5$ cm^{-1}.

Figure 7 shows for 3-GHz frequency, the variation of the amplification rate of the surface phonons with propagation direction on the (001) plane. The amplification rate of the phonons corresponding to the PSW is shown by the cross. It can be seen that the surface phonons of the normal branch couple to the electrons through piezoelectricity most strongly at an angle around 22.5°, which is almost identical to the pure-mode axis. We also see that the surface phonons of the pseudo branch interact with the electrons more strongly than the phonons of the normal branch.

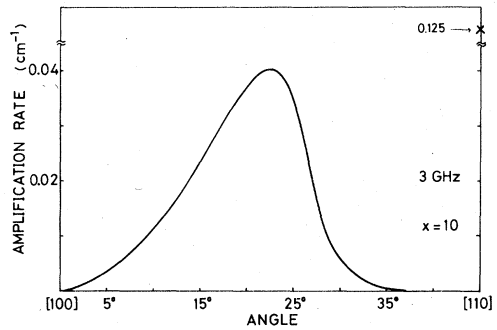

FIG. 7. Angle dependence of the calculated amplification rate of surface phonons for 3-GHz frequency and for drift parameter $x = 10$. The cross at 45° indicates the amplification rate of the surface phonons of the pseudo branch.

This calculated angle dependence is quite dissimilar to that of the isotropic approximation. We note that the latter grows as $(\kappa_1\kappa_2)^2 \propto \sin^2 2\theta$, where θ is the angle rotated from the crystal axis.[3] Furthermore, for 3-GHz frequency the amplification rate of the isotropic approximation reaches up to 0.579 cm^{-1} at $\theta = 45°$, whereas Fig. 7 tells us that the maximum amplification rate is 0.125 cm^{-1} for the same frequency if the anisotropy effects are taken into account. This significant reduction of the amplification rate can be explained by the oscillation in the depth dependence of the induced potential for the anisotropic medium, that is, the oscillation implies that the orientation of the electric fields accompanying the acoustic fields rotates with the depth and hence it yields a partial cancellation of the effective magnitude of the electric fields to which the electrons are coupled. It should be noted that as far as the (001) plane of the cubic crystal is concerned, this calculated curve for the amplification rate is common to all piezoelectric semiconductors with $\eta > 1$. On the other hand, for semiconductors with the same symmetry but with $\eta < 1$, the angle dependence of the amplification rate on the same plane is expected to manifest a rather similar behavior to that of the isotropic semiconductors ($\eta = 1$) mentioned above, apart from overall magnitude.[18]

Figures 8(a) and (b) display the frequency dependences of the amplification rate at 22.5 and 45° (pseudo branch), respectively. For the sake of comparison, the amplification rates obtained by assuming the absence of the depletion layer ($l_0 = 0$) (dot-dash line), and nonexistence of the electrons for $x_3 < l_0$ (broken curve) are drawn simultaneously. The former is proportional to ω^3 for frequencies corresponding to wave number k satisfying $k << k_s$. We also find that the electrons which extend over the region $x_3 < l_0$ act to shift higher the frequencies at which the local extrema of the amplification rate are reached as well as to make the overall magnitudes of the amplification larger. These characteristics have been equally found for Rayleigh waves. However, when the existence of the electron depletion layer is introduced, the frequency dependence of the amplification rate is modified even qualitatively. Here, we remember that the amplification rate of the surface phonons obtained in the isotropic approximation has two bumps and a dip for certain frequencies between

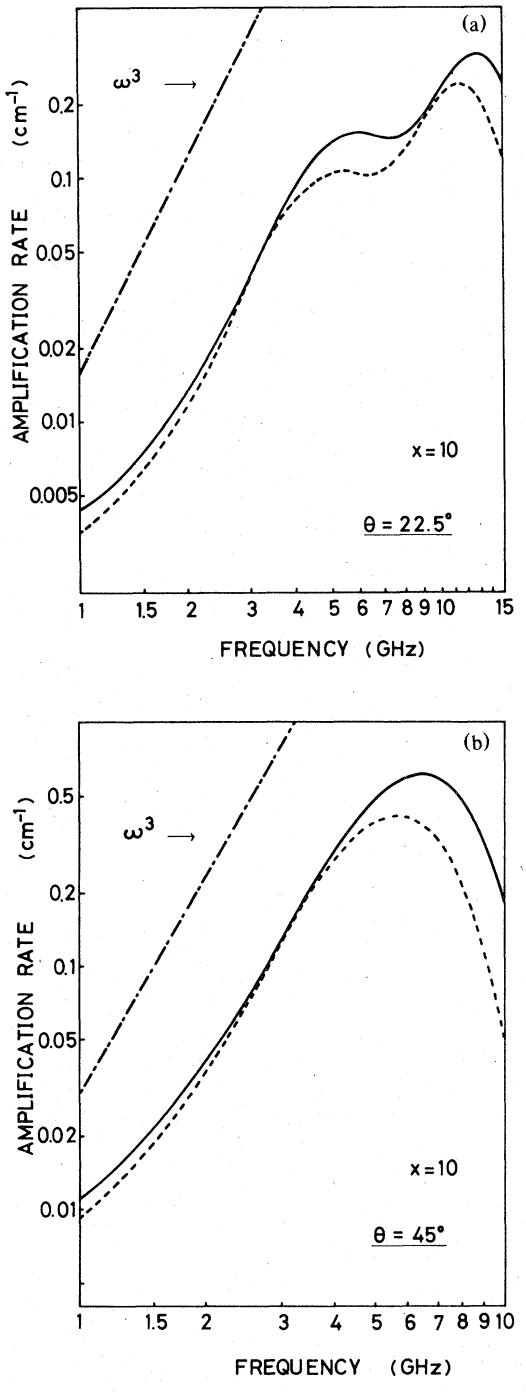

FIG. 8. Frequency dependence of amplification rate for propagation at 22.5° (a), and 45° (pseudo branch) (b), rotated away from the [100] axis in the (001) plane, and for drift parameter $x = 10$. The broken curves give the amplification rate calculated by assuming no electrons for $x_3 < l_0$. The dot-dash lines represent an amplification rate proportional to ω^3 and are obtained when the depletion layer is ignored, i.e., $l_0 = 0$.

1 and 10 GHz. The existence of both the bumps and the dip has been understood approximately by the $\vec{k}$ dependence of the following quantity[3]:

$$Y_{\vec{k}} = \frac{k^4}{(k^2 + k_s^2)^2} \left| \int_{l_0}^{\infty} \phi_{\vec{k}}(x_3)\, dx_3 \right|^2 , \tag{61}$$

where $\phi_{\vec{k}}(x_3)$ is defined by

$$\phi_{\vec{k}}(\vec{r}) \equiv \phi_{\vec{k}}(x_3) e^{i\vec{k}\cdot\vec{x}} . \tag{62}$$

In this approximation, the appearance of the dip corresponds to the vanishing of $Y_{\vec{k}}$ for an appropriate $\vec{k}$.

At 22.5°, two bumps and a dip appear in the frequency region 1–15 GHz and for higher frequencies the amplification rate decreases exponentially. These characteristics seem to be qualitatively very similar to those of the isotropic approximation apart from the values of the frequencies at which the local extrema are reached. This close resemblance is, nevertheless, just an apparent one, as will be explained right below. At 45°, only one local maximum can be seen in the GHz-frequency region. The spatial behavior of the potential perpendicular to the surface (Fig. 6) and Eq. (61) help us to establish that this maximum corresponds to the lower frequency one for 22.5° and to the higher frequency one in the isotropic approximation.[3] More precisely, up to about 15-GHz phonon frequencies, there could be three and two bumps for 22.5 and for 45°, respectively, provided the interpretation of the amplification on the basis of Eq. (61) is valid for all frequencies. After a careful consideration of the induced potential (Fig. 6), we can conclude that the oscillation of the potential characteristic to elastic anisotropy is responsible for the occurrence of the local maxima or minima of the amplification rate at frequencies higher than 10 GHz. The oscillation of the potential with depth is really striking for 22.5° and it generates the bump above 10 GHz observed in Fig. 8(a). On the other hand, the oscillation is inconspicuous for the PSW's (rather similar to the Rayleigh waves) and then the other bumps at high frequencies (>10 GHz), if present, will not be detected being practically screened by the rapid exponential decrease of the amplification.

Equation (61) tells us that the other bump in the amplification rate, corresponding to the lower-frequency one in the isotropic approximation, may exist at frequencies lower than 1 GHz. Unfortunately, our approximation fails even qualitatively at such low phonon frequencies. In both Figs. 8(a) and (b), we only see a gentle growth of the amplification rate at frequencies near 1 GHz. In conclusion, owing to the presence of the elastic anisotropy of the semiconductor, the amplification rate of the surface phonons generally has additional bumps and dips in its frequency dependence, which do not have counterparts in isotropic semiconductors.

VIII. CONCLUSIONS

In this paper, we have investigated the acoustoelectric interaction of the surface phonons in piezoelectric semiconductors taking the effect of elastic anisotropy into account. Since the anisotropy introduces some quantitative changes on the underlying SAW theory in the isotropic approximation, the interaction has been expected to suffer the considerable effects of these. The oscillation in the decay of the particle displacement away from a solid surface is one of the most remarkable alterations caused by anisotropy. We have seen that this oscillation brings about significant reduction of the coupling strength between the electrons and the surface phonons as compared with the isotropic approximation. However, the magnitude of the interaction is still large enough to be detected experimentally.

The oscillatory behavior of the particle displacement with depth causes qualitative changes as well in the frequency dependence of the attenuation or the amplification rate of the surface phonons when the thickness of the depletion layer at the semiconductor surface becomes of the same order of magnitude as the wavelength of the surface phonons. It may be noteworthy that no notable changes are present apart from the overall magnitude of the amplification if the existence of the depletion layer at the semiconductor surface is neglected.

Another relevant characteristic introduced for the surface phonons by the anisotropy is that there exist generally three independent components of the particle displacement and their relative magnitude (and then the polarization of the phonons) varies with the direction of propagation. The variation of the attenuation or the amplification rate of the surface phonons with their propagation direction is closely connected with this property of the phonons in the anisotropic media because the electrons interact with the surface phonons through the induced longitudinal electric field whose strength is sensitively dependent upon the polarization of the phonons. The calculated angle dependence of the amplification is different even qualitatively from that of the isotropic approximation, where only two independent components of the particle displacement are present for the Rayleigh waves.

In this paper we have made some simplifications as in Paper I, that is, we have approximated the relaxation time of the electrons to be infinite and we have ignored the contributions of the electrons in the region $x_3 < l_0$ to the electronic screening. Somewhat detailed discussions of these points have already been given in Paper I. Here, we only remark that our approximations do not prevent us from understanding the crucial effects of elastic anisotropy on the acoustoelectric interactions of the surface phonons in semiconductors.

ACKNOWLEDGMENTS

The author would like to express his sincere thanks to Professor T. Sakuma for checking the calculations and carefully reading the manuscript. He also thanks the Sakkokai Foundation for financial support. This work is also supported by the Scientific Research Fund from the Ministry of Education. The numerical calculations were performed using the FACOM 230-75 facilities at the Hokkaido University Computing Center.

---

[1]J. R. Sandercock, Solid State Commun. 26, 547 (1978); N. L. Rowell, V. C. Y. So, and G. I. Stegeman, Appl. Phys. Lett. 32, 154 (1978); N. L. Rowell and G. I. Stegeman, Phys. Rev. Lett. 41, 970 (1978).

[2]S. Tamura and T. Sakuma, Phys. Rev. B 15, 4948 (1977); 1977 Ultrasonics Symposium Proceedings, IEEE Cat. No. 77 CH 1264-1SU (unpublished), p. 301.

[3]S. Tamura and T. Sakuma, Phys. Rev. B 18, 5514 (1978).

[4]G. W. Farnell, in *Physical Acoustics,* edited by W. P. Mason and R. N. Thurston (Academic, New York, 1970), Vol. 6, p. 109.

[5]G. W. Farnell, in *Acoustic Surface Waves,* edited by A. A. Oliner (Springer, New York, 1978), p. 13.

[6]See, for example, H. N. Spector, in *Solid State Physics,* edited by F. Seitz and D. Turnbull (Academic, New York, 1966), Vol. 19, p. 291.

[7]J. L. Bleustein, Appl. Phys. Lett. 13, 412 (1968).

[8]C.-C. Tseng, Appl. Phys. Lett. 16, 253 (1970).

[9]J. J. Campbell and W. R. Jones, J. Appl. Phys. 41, 2796 (1970).

[10]S. Tamura (unpublished).

[11]M. Neuberger, *Handbook of Electronic Materials* (Plenum, New York, 1972), Vol. 2.

[12]The characteristics of the SAW in the anisotropic medium with $\eta < 1$ are somewhat different from those of the materials with $\eta > 1$, especially in the velocity curves. See, Ref. 4.

[13]SAW's propagating along the $[1\bar{1}0]$ direction on the (110) surface are simple Rayleigh waves, that is, the particle displacement is in the sagittal plane and no oscillation appears in its decay profile. Also no piezoelectric effects are present for the SAW's traveling in this configuration.

[14]In the anisotropic half space, there exist the solutions of Eq. (11) with Eq. (7) which break the translation invariance in the directions parallel to the surface. These are pseudo surface waves in the usual sense (which should not be confused with the PSW's used in this article exclusively as true surface waves in the pseudo branch). The pseudo surface waves are characterized by the presence of small imaginary parts (typically of the order of 10^{-4}) in the direction cosines (κ_1, κ_2) and $\kappa_3^{(3)}$, and they attenuate in the direction normal to the surface wave

fronts ($\mathrm{Im}\kappa_1 = \mathrm{Im}\kappa_2 > 0$) but blow up at infinite depth ($\mathrm{Im}\kappa_3^{(3)} < 0$). Accordingly, the operators $\tilde{L}(\partial)$ cannot be Hermitian, as it stands, on the space of the pseudo surface waves with scalar products defined by Eqs. (19) and (20). However, because of the smallness of the imaginary parts mentioned above, the pseudo surface waves behave very much like the SAW's for propagation over finite depths. Therefore, as far as we consider the displacement of the medium near the surface, we may consider that the acoustic waves including the pseudo surface waves make approximately the operator $\tilde{L}(\partial)$ Hermitian. In order to quantize more rigorously the acoustic waves in the anisotropic half space, we may begin by defining the scalar products in a slightly different manner from Eqs. (19) and (20) such that they converge for pseudo surface waves and the Hermiticity of the operator $\tilde{L}(\partial)$ is guaranteed.

[15]See, for example, A. Many, Y. Goldstein, and N. B. Gover, *Semiconductor Surfaces* (North-Holland, Amsterdam, 1971).

[16]F. Stern and W. E. Howard, Phys. Rev. 163, 816 (1967).

[17]Hereafter, we take the unessential normalization area S to be unity.

[18]This can be expected from the velocity variation of the SAW's. See, for example, Ref. 9.